Endohedral adsorption in graphitic nanotubules

J. Breton, J. GonzalezPlatas, and C. Girardet

Citation: The Journal of Chemical Physics **101**, 3334 (1994); doi: 10.1063/1.467581
View online: http://dx.doi.org/10.1063/1.467581
View Table of Contents: http://scitation.aip.org/content/aip/journal/jcp/101/4?ver=pdfcov
Published by the AIP Publishing

Endohedral adsorption in graphitic nanotubules

J. Breton and J. Gonzalez-Platas
Departamento de Fisica Fundamental y Experimental-Universidad de La Laguna, 38203 Tenerife, Spain

C. Girardet
Laboratoire de Physique Moléculaire, URA CNRS 772, UFR Sciences et Techniques, La Bouloie, Université de Franche-Comté, 25030 Besançon Cedex, France

(Received 21 March 1994; accepted 25 April 1994)

Calculations based on simple interaction potentials are performed to define the adsorption characteristics of molecules encapsulated in carbon nanotubules. The continuum approximation used to describe the cylindrical sheets is shown to work fairly well within a large range of tubule diameters. Criteria for molecule confinement are given which include the influence of the number of graphitic shells describing the whole tubule and they are compared to similar results obtained for carbon Buckyballs. Application to the most common encaged species, i.e., rare gas atoms and alkali-metal ions, confirms these general rules.

I. INTRODUCTION

The synthesis of molecular carbon structures in the form of C_{60} and other fullerenes[1] has led to the recent preparation[2] of a new type of nanostructures consisting of needlelike tubes with mesoscopic length (up to 10^4 Å). Each needle comprises coaxial tubes of graphitic sheets and the carbon hexagons are arranged in a helical fashion about the needle axis. Wall thicknesses of the tubules range from 2 to 50 sheets and the outer diameter of the needles can vary from 40 to 300 Å. The structure of these hollow graphitic tubules has been confirmed[3] using variants of the standard synthesis technique. High-resolution electron micrographs and x-ray diffraction patterns[3,4] have revealed that the mean distance between coaxial graphitic sheets is about 3.44 Å, roughly the same as between graphite planes (3.4 Å).

Very recently, the synthesis of abundant single-shell tubes, which grow in the gas phase instead of being formed on the carbon cathod, has been reported.[5,6] The diameters of individual tubules have been measured[5] on the electron micrographs and the histogram for the inner diameters shows two peaks around 8 and 10.5 Å. With such dimensions, these tubules are thus ideal candidates to encapsulate molecules.

The possibility of encapsulating molecules inside fullerene cages is now strongly supported by a growing body of experimental evidence, mainly for the production of metallofullerenes and also for rare-gas and even small diatomic molecules like CO, encaged in Buckyballs.[7] It appears that the carbon nanotubes are invariably capped at their ends and an efficient encapsulating process requires the destruction of the tube caps. An oxidation technique can be used[8,9] to produce thinner tubes and to destruct the caps; as a result, the opened tubes can be regarded as nanoscale test-tubes for adsorption of molecules. Filling of the interior of the tubes with an inorganic phase has led to much speculations about the possible uses of these graphitic structures. Capillarity-induced filling of the tubes with molten material has been shown[10] to be efficient in a one-step process from closed tubes. However, it is not well understood whether the second-step encapsulating, from open tubes, is a complicated phenomenon for very thin tube diameters, whereas it appears as an easier process for much larger nanotubes.[11,12]

From a theoretical point of view, these carbon needles have stimulated intense interest through their structural and physical (electronic and magnetic) properties. The energetical stability of microtubes has been investigated using Tersoff's potential calculations[13] and tight-binding approaches[14] to estimate the deformation and stitching energies. In both cases, predictions of extremely thin tubes have been done, with diameters less than 4 or 6 Å. Moreover, the atomic structure of these tubules in terms of helical arrangement of the carbon hexagons has been discussed[15–19] in order to specify the symmetries and it has been shown that two integer numbers m and n allow the geometrical specificity of the tubules to be uniquely determined. Implications on the metallic or semiconducting behavior of the tubules[20–23] can then be studied for the three main structures corresponding to armchair, zig–zag, and chiral arrangements.[18,19]

Recent emphasis has been also given to the computation using an expanded Hückel method[24] of the electron structure of tubelenes $X@C_{m,n}$ where X defines a metal atom and $C_{m,n}$ a single-shell nanoscale tube with a geometry specified by the integers m and n. It is shown that these nanotubes change from semimetal character to metal due to alkali-metal ion doping. Fullerene tubes have been furthermore considered[25] as highly-polarizable molecular straws capable of ingesting molecules. Local density functional calculations have been performed[25] on HF molecules constrained to move along a tubule axis and they are expected to open the way to the study of nanoscale capillarity.

In this paper, we study some basic properties related to the endohedral or exohedral adsorption of atoms or ions in fullerene tubes. The interaction potential between a molecule and a graphitic tubule is approximated through a continuum description of the mesoscopic system. The conditions for the application of such an approach are given in terms of a minimum set of parameters including the potential coefficients and the tube diameter. Criteria for exohedral or endohedral adsorption and then for axial confinement of the molecule inside the tube are established, leading to some general conclusions on the encapsulating specificity of the fullerene tu-

 0021-9606/94/101(4)/3334/7/$6.00

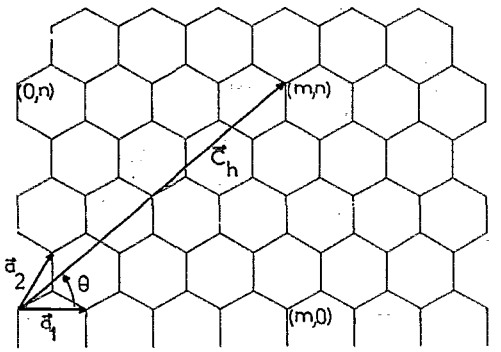

FIG. 1. Atomic structure of microtubules constructed from the rolled graphitic sheet. Vectors $\mathbf{a}_1$ and $\mathbf{a}_2$ are unit vectors of the two-dimensional lattice and $\mathbf{C}_h$ indicates the direction perpendicular to the cylinder axis (the head and tail of $\mathbf{C}_h$ coincide when the sheet is rolled). The coordinates of some lattice points is given as the set (m,n) of integer numbers.

bules. Application to the inclusion of rare gas atoms and alkali-metal ions is presented.

II. STRUCTURE AND INTERACTION POTENTIAL

Each nanotube can be visualized as a conformal mapping of two-dimensional honeycomb graphite lattice onto the surface of a cylinder subject to periodic boundary conditions around the cylinder and along its symmetry axis. Every graphitic lattice vector $\mathbf{C}_h$ can be defined in terms of two primitive lattice vectors $\mathbf{a}_1$ and $\mathbf{a}_2$ (Fig. 1) and of a pair of integer numbers m and n as

$$\mathbf{C}_h = m\mathbf{a}_1 + n\mathbf{a}_2. \tag{1}$$

We adopt the construction scheme and notation of Refs. 17 and 19. Thus, a cylindrical tube $C_{m,n}$ is characterized by its radius $R_{m,n}$,

$$R_{m,n} = \frac{\sqrt{3}a}{2\pi}(m^2+n^2+mn)^{1/2}, \tag{2}$$

where $a = 1.42$ Å is the carbon–carbon nearest-neighbor distance in the graphitic surface, and by the chiral angle θ which defines the different ways of rolling up the graphite sheet in Fig. 1,

$$\theta = \mathrm{Arctan}[\sqrt{3}n/(2m+n)]. \tag{3}$$

Nanotubes with m or $n=0$ and with $m=n$ are not chiral and correspond to zig–zag or armchair geometries while general values for $m \neq n \neq 0$ lead to the missing of a reflection plane involving chirality.

The tubules are assumed to be rigid and not deformed by molecular endohedral or exohedral adsorption. The interaction potential between the admolecule X and a carbon atom pertaining to the network is written as a Lennard-Jones form with parameters ϵ and σ,

$$v = \sum_{k=6,12} \frac{(-1)^{k/2} 4\epsilon\sigma^k}{d^k}, \tag{4}$$

where d characterizes the distance between the centers of mass of the two particles. The total potential is then a sum of these pairwise contributions. Within the continuum description of the nanotubule, this total potential can be written in terms of reduced quantities as

$$V^* = \frac{8\pi}{3\sqrt{3}a^{*2}} \sum_{k=6,12} G_k(s)/R^{*k-2}, \tag{5}$$

with $V^* = V/\epsilon$, $R^* = R/\sigma$, and $a^* = a/\sigma$. R defines the radius of the cylinder. The curvature functions $G_k(s)$ depend only on the reduced distance $s = r/R$, where r characterizes the distance between the X molecule location and the cylinder axis. These functions are given by

$$\begin{aligned} G_{12}(s) = \frac{1}{160(1-s)^2(1+s)} \Bigg\{ E(q) \Bigg[& \frac{128}{(1+s)^8} + \frac{104}{(1-s)^2(1+s)^6} + \frac{99}{(1-s)^4(1+s)^4} \\ & + \frac{104}{(1-s)^6(1+s)^2} + \frac{128}{(1-s)^8} \Bigg] \\ & - \frac{4K(q)}{(1+s)^2} \Bigg[\frac{16}{(1+s)^6} + \frac{15}{(1-s)^2(1+s)^4} \\ & + \frac{15}{(1-s)^4(1+s)^2} + \frac{16}{(1-s)^6} \Bigg] \Bigg\} \end{aligned} \tag{6}$$

and

$$G_6(s) = \frac{1}{(1-s)^2(1+s)^3} \left[4E(q) \frac{(1+s)^2}{(1-s)^2} - K(q) \right]. \tag{6'}$$

The ellyptic integrals $E(q)$ and $K(q)$ of first and second species[26] depend on the reduced variable q defined as

$$q = 2\sqrt{s}/(1+s). \tag{7}$$

Note that the condition $s<1$ implies that the molecular adsorption is endohedral ($X@C_{m,n}$) whereas $s>1$ corresponds to exohedral adsorption ($@C_{m,n}X$). However, in both situations, one has $q<1$. Moreover, for $s=0$, the molecule remains confined along the tubule axis and the corresponding functions $G_k(0)$ take quite simple constant values

$$G_{12}(0) = \frac{63}{64}\pi$$

and

$$G_6(0) = \frac{3}{2}\pi. \tag{8}$$

It can be mentioned that Eqs. (5), (6), and (6′) are another analytic form of the interaction energy calculated for an atom in a pore,[27] using an even power series expansion with respect to s.

III. EQUILIBRIUM AND STABILITY FOR THE ADSORPTION SITES

The equilibrium position of the X molecule is simply determined by differentiating Eq. (5) with respect to s. The first root $s_1 = 0$ corresponds to minimum or maximum energy values depending on R^* is smaller or larger than R_1^*

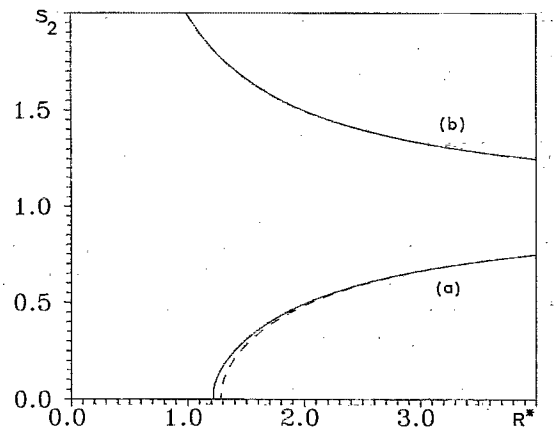

FIG. 2. Behavior of the s_2 root of the interaction potential vs the reduced tubule radius R^* for endohedral (a) and exohedral (b) adsorption of the X molecule in a continuum tubule (full curve) and in a spherical fullerene (broken line).

$\simeq (105/32)^{1/6} \simeq 1.22$. This latter value is a characteristic of the potential form used here and defines the condition for the molecular confinement in a nanotubule, in terms of the ratio of the cavity radius and of the molecular Lennard-Jones diameter.

On the contrary, the behavior of the second root s_2 depends strongly on the R^* values and on the endohedral or exohedral nature of the X adsorption (Fig. 2). The endohedral root decreases with R^* down to the axial confinement condition is reached, whereas the exohedral root naturally increases when R^* decreases. For large R^* values, the two curves tend toward the same asymptotic value $s=1$ since the cylinder behaves as a graphitic plane with equivalent adsorption sites on each side of this plane.

Figure 3 exhibits the behavior of the minimum interaction potential $V^*(s_2)$ as a function of the reduced radius of the nanotubule. When the molecule is adsorbed outside the nanotubule, the potential energy minima monotonously increase when R^* decreases and they reach a zero value at $R^*=0$. This behavior can be easily understood since the asymptotic situation $R^*=0$ corresponds to a linear distribution of continuum matter for the tube with a linear reduced density ρ_l^* proportional to R^*,

$$\rho_l^* = \frac{8\pi R^*}{3\sqrt{3}Na^{*2}}, \tag{9}$$

where N defines the number of carbon atoms along the circumference of radius R^*. The interaction potential is then written as

$$V^* = \frac{3\pi}{2} N \frac{\rho_l^*}{r^{*5}} \left(\frac{21}{32 r^{*6}} - 1 \right) \tag{10}$$

and it vanishes when the cylinder radius tends to zero.

The exohedral adsorption is stable up to $R^*=0.94$. When R^* becomes larger, the stable adsorption sites are calculated inside the tubule. The minimum potential curve strongly decreases and reaches an absolute minimum for $R_M^* \sim 1.09$. It then increases with R^* and tends to an asymptotic value which is common to the exohedral curve for large R^* values. This common value V_C^* is given by

$$V_C^* = -\frac{8\pi}{5\sqrt{3}a^{*2}}. \tag{11}$$

It defines the interaction between the admolecule and the graphitic continuum plane which can be reached both from the endohedral and the exohedral situations when R^* is infinite.

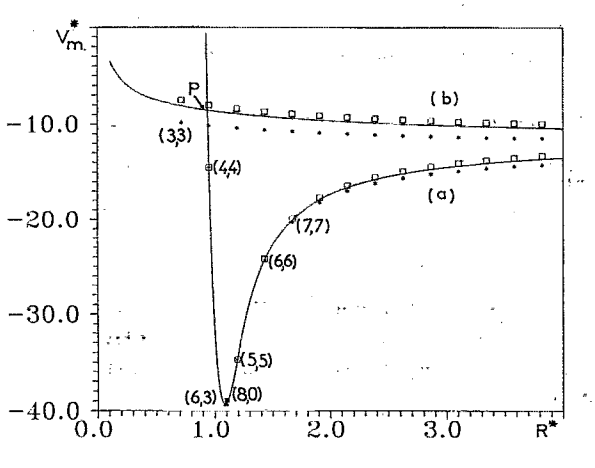

FIG. 3. Minimum interaction potential V_m^* (in reduced unit) for the admolecule vs the reduced tubule radius R^*, for endohedral (a) and exohedral (b) adsorption. Full curves correspond to the continuum approximation; stars and squares characterize the equilibrium potential in discrete $C_{m,n}$ tubules when the molecule moves toward the center of a carbon hexagon (free to matter) or toward a carbon atom. Point P at the intersect of curves (a) and (b) represents the stability boundary for endo and exohedral adsorptions.

IV. COMPARISON BETWEEN THE DISCRETE AND CONTINUUM APPROACHES

In Fig. 3, beside the full curves associated with the potential minima within the continuum approximation, we give the corresponding values determined by minimizing the total potential obtained from a discrete pairwise sum. Two situations are considered according to the admolecule is adsorbed along an axis perpendicular to the tubule axis which contains carbon atoms or along an axis intersecting the center of a graphitic hexagon. The calculations have been performed for various tubules $C_{m,n}$ but, for clarity, we have mainly represented the results for the armchair geometries. Indeed, the values of the minima connected to zig–zag and chiral geometries are very close to those for the armchair structures having a similar reduced radius. We see that the discrete and continuum approaches give nearly identical results (with an accuracy better than 1%) for the endohedral adsorption when $0.94 \leq R^* \lesssim 1.90$. For larger R^* values, the situation for which the admolecule moves toward an hexagon center appears always more stable than the other, the continuum approximation leading to intermediate results. In contrast, this continuum approximation is less accurate for the exohedral adsorption because it underestimates the potential minimum, whatever R^*.

Further examination of the results in Fig. 3 allows us to classify the adsorption properties as a function of the tubule radius.

(i) When $R^* \lesssim 0.94$, the exohedral adsorption is the most stable. It is obtained for the following thin and non chiral tubules $C_{3,3}$, $C_{5,0}$, and $C_{6,0}$. These tubules are those which have been found to be stable[13] using Tersoff's potential to describe carbon–carbon interactions. As already mentioned, the continuum approximation does not work well since it underestimates the potential minimum by about 10%.

(ii) When $0.94 \lesssim R^* \lesssim 1.22$, the endohedral adsorption becomes more stable and the admolecule remains confined along the tubule axis. Only the chiral tubes $C_{6,2}$ and $C_{6,3}$ and the achiral tubes $C_{4,4}$, $C_{5,5}$, $C_{7,0}$, and $C_{8,0}$ satisfy this condition. It may be furthermore noted that the adsorption is optimized with the $C_{6,3}$ geometry (see Fig. 3). The $C_{5,5}$ tube is the thinnest graphite filament which is calculated to be stable using tight-binding electronic calculations.[14] For all these tubules, the continuum approximation is quite valid.

(iii) When $1.22 \lesssim R^* \lesssim 1.90$, the continuum approximation is still valid but the center of mass of the admolecule is not confined along the axis. Such a situation is obtained for the achiral tubules $C_{6,6}$, $C_{7,7}$, and $C_{8,8}$ since the accuracy is better than 1% on the energy as well as on the equilibrium position of the molecule.

(iv) When $R^* \gtrsim 1.90$, the inaccuracy significantly increases on the position of the admolecule (~20%) while it remains reasonable on the value of the minimum energy (~2%).

Beside, the reduced energy difference $\Delta V^* = V^*(0) - V_m^*$ has been calculated for the endohedral adsorption as a function of R^*; $V^*(0)$ and V_m^* characterize the values of the potential energy along the tubule axis and at the equilibrium, respectively. This difference strictly vanishes when $0.94 \lesssim R^* \lesssim 1.22$ due to the axial confinement and then strongly increases up to 13.3 for a value $R^* = 3.07$. It then reaches a nearly constant value for larger R^*, as expected for the interaction between the admolecule and the continuum graphitic plane. The reduced distance r^* of the molecule to the tubule axis increases in a nonlinear way from 0 up to 1 when R^* increases from 1.22 to 1.9 and it then has a linear behavior with R^* since the influence of curvature tends to cancel.

V. COMPARISON BETWEEN THE TUBULE AND SPHERE ADSORPTION

At this stage, it can be mentioned that these results are rather general since they only depend on the form of the pairwise potential used to describe the interaction between the molecule and a carbon atom. Such results can thus be compared to those obtained[28] for a similar adsorption process inside and outside a carbon sphere (Buckyball) of radius R^*, with the same areal carbon density. The value $R_1^* = 1.28$ for the sphere is larger than that calculated for the tubule ($R_1^* = 1.22$), thus indicating that the confinement of the admolecule at the sphere center is an easier process than along the cylinder axis. The curvature differences for the sphere and the cylinder appear also significant on the stability of the outside and inside molecular adsorptions, since $R_M^* = 1.01$ for the sphere against $R_M^* = 0.94$ for the tubule. Figure 2 shows this influence for the endohedral root (broken curve) while the difference between the tube and the sphere is negligible for the exohedral root. It can be easily demonstrated that the absolute minimum for the molecule–sphere interaction is lower than for the corresponding tubule when $R^* \gtrsim 1.065$. The energy difference between the sphere and the tube is maximum for $R^* \simeq 1.85$ where it reaches 29% of the well depth.

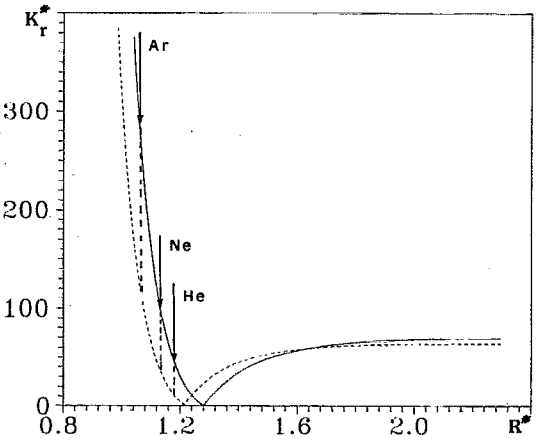

FIG. 4. Behavior of the reduced radial force constant $k_r^* = (d^2V^*/dr^2)$ ($Å^{-2}$) within the continuum approach for a sphere (full curve) and a cylinder (broken curve) vs the reduced radius R^*. Arrows correspond to the values of $k_r^*(R^*)$ for the three endohedral rare gas atoms He, Ne, and Ar (see also Table V).

Figure 4 exhibits the behavior of the radial force constant k_r^* for the admolecule inside a spherical fullerene and a tube with the same radius and areal density as a function of the reduced radius R^*. The value of k_r^* is smaller for the cylinder than for the sphere when $R^* \lesssim 1.235$. It can be noted that such a R^* value corresponds to a confinement of the molecule at the sphere center ($R^* \lesssim 1.28$) whereas the position of the molecule can lie outside the tube axis for $R^* \gtrsim 1.22$. When $1.235 \lesssim R^* \lesssim 1.635$, the force constant k_r^* remains small for both cases, indicating rather flat potential wells but it is larger for the cylinder. For much larger R^* values, the asymptotic behavior is obtained, which corresponds to the graphitic plane. We can therefore conclude that the radial confinement is more efficient in the sphere with sharper wells when $R^* \lesssim 1.235$.

VI. CONFINEMENT IN MULTISHELL NANOTUBES

All the previous results are obtained for a single-shell carbon nanotube. However electron microscopy reveals carbon structures consisting of needlelike tubes containing a number of coaxial graphitic sheets between 1 up to about 50. The aim of this section is to calculate whether a molecule can be adsorbed between successive cylindrical sheets or, on the contrary, can only be confined inside the first cylindrical

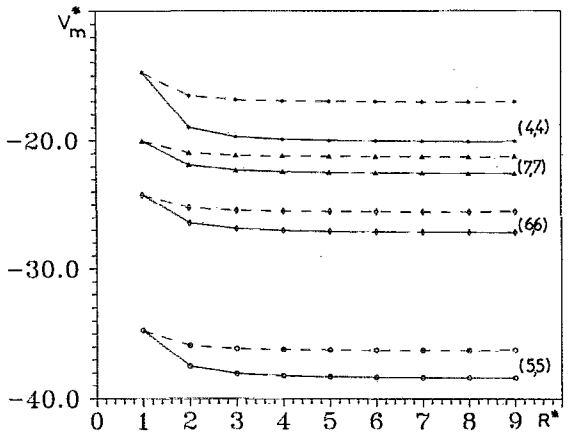

FIG. 5. Minimum interaction potential V_m^* (in reduced unit) for the admolecule vs the shell number N of the graphitic tubule. Full curves correspond to accurate values for tubule diameters obeying the continuum approximation. Broken curves characterize the planar sheet approximation. The difference between the two series of curves is a characteristic of the geometrical confinement induced by the multishell tubules.

cavity. In this second situation, it is also interesting to determine the influence of the sheet number on the adsorption characteristics.

We assume that a tube is formed by a set of coaxial cylindrical continuum sheets at a distance $L=3.44$ Å given by experiments.[3,4] The reduced radius R^* of the internal cylinder can be varied, as in the previous sections. Using Eq. (5), we have calculated the minimum distance L_0^* leading to a negative value for the interaction potential of an admolecule located between two cylindrical sheets of a carbon tube. The value $L_0^* = 1.71 \pm 0.1$ is nearly independent from the sheet number in the tube and from the internal radius R. The interaction potential is optimized when the sheet distance is $L_M^* = 1.995$. Such a value appears to be very close to the optimized distance D^* leading[29] to a minimum adsorption energy for a molecule between two continuum graphitic planes ($D^*=2$). However, both values L_0^* and L_M^* appear much larger than the physical values obtained for most of adatoms and admolecules ($L^*<1.5$) and we can conclude that the intershell adsorption is not stable. Such a result agrees with experimental observations.[10]

Since adsorption proceeds only inside the internal cylinder, we have calculated the equilibrium position of the admolecule and the corresponding interaction energy, within the continuum approximation for various multishell tubules. This equilibrium position does not significantly depend on the sheet number N (less than 1%) and is a characteristics of R^*, only. On the contrary, Fig. 5 shows that the adsorption energy is significantly influenced by N since it decreases by about 33% for the thinnest tube $C_{4,4}$ and by 13% for the tube $C_{7,7}$ for which the continuum approximation is still valid. In all cases, the first four shells contribute to this decrease whereas the influence of the highest shells is negligible. For comparison, we have also drawn in Fig. 5 the energy curves obtained by assuming that all the sheets excepted the first one are planar instead of being cylindrical. The effect is less pronounced, and we can therefore conclude that the adsorption in cylindrical multishell tubules is favored with respect to the single sheet tubes by the number and the curvature of the graphitic sheets. This is a consequence of the geometrical confinement which can be evidenced through another feature. Indeed, it can be mentioned that the multishell structures for which the axial confinement of the admolecule is not verified ($C_{6,6}$, $C_{7,7}$, $C_{8,8}$,...) tend to decrease the energy difference ΔV^* by about 10%. A planar sheet model would in contrast lead to an increase of ΔV^*.

TABLE I. Lennard-Jones parameters. The parameters for the heterogeneous pairs are obtained by applying the usual combination rules (Ref. 28).

X	C	Li^+	Na^+	K^+	He	Ne	Ar	Kr	Xe
σ (Å)	3.50	2.10	2.50	2.93	3.03	3.18	3.46	3.55	3.83
ϵ (meV)	2.1	74.4	43.6	28.0	1.4	2.2	7.7	5.3	6.3

VII. APPLICATION TO THE ADSORPTION OF RARE GAS AND ALKALI-METAL ATOMS

The endohedral adsorption of rare gas atoms and alkali-metal ions has been applied to single-shell and multishell carbon tubules with radii $R=5.25$ and 4.0 Å. Such tubules are the most stable needles observed in electron micrographs.[5] In Table I, we give the values of the potential parameters used in our calculations. Let us mention here that a Lennard-Jones potential can appear much too crude for an accurate description of the interactions between a graphite network and an atom. There is in fact a large body of work concerned with interactions with the flat graphite surfaces.[30–32] Improved forms of potentials could be used in further studies, but the main emphasis of the present model lies on the simplicity of analytic calculations and therefore restricts the use of sophisticated and less tractable potential descriptions. The values of a^* and L^* required for the application of the continuum model are presented in Table II. Note that the values L^* are smaller than $L_0^* = 1.71$ determined in Sec. VI.

The results of calculations for the two species of tubules are reported in Tables III and IV. For each adatom, we calculate the values of R^*, of the equilibrium position r_m of the adatoms with respect to the tubule axis, the corresponding minimum energy V_m for a single-shell and a four-shell tubule and the energy difference ΔV.

Since $R^*>1.22$, all the atoms considered here are not confined along the tubule axes with $R=5.25$ Å (Table III). Moreover, for the Li^+ and Na^+ ions, the continuum approximation is not strictly valid, as shown in Fig. 3, although the inaccuracy remains weak for the adsorption energy. The minimum energy appears to be large for the alkali-metal ions, with a high radial potential barrier ΔV which is maxi-

TABLE II. Parameters for the continuum approximation.

X	Li^+	Na^+	K^+	He	Ne	Ar	Kr	Xe
$a^*=a/\sigma$	0.676	0.568	0.485	0.469	0.447	0.410	0.400	0.371
$L^*=L/\sigma$	1.62	1.36	1.16	1.12	1.07	0.98	0.96	0.89

TABLE III. Adsorption characteristics for various atoms in a carbon tubule with radius 5.25 Å.

			V_m (meV)		$\Delta V = V(0) - V_m$ (meV)		
X	R^*	r_m (Å)	$N=1$	$N=4$	$N=1$	$N=4$	ω_r (cm^{-1})
Li^+	2.50	3.13	−628	−702	533	575	444
Na^+	2.10	2.72	−568	−637	411	440	182
K^+	1.79	2.26	−560	−629	301	321	110
He	1.73	2.26	−31	−35	15	16	76
Ne	1.65	1.99	−56	−63	23	25	42
Ar	1.52	1.68	−156	−175	43	46	42
Kr	1.48	1.57	−191	−215	44	47	23
Xe	1.37	1.21	−298	−333	31	34	5

mum along the tubule axis. Note the influence of the shell number on the magnitude of this barrier, since the minimum energy decreases by 12% when N increases while the barrier increases by only 7%.

When the tubule radius decreases ($R=4.0$ Å, Table IV), all the atoms satisfy the validity of the continuum approximation. Moreover, the three heaviest rare gas atoms (Ar, Kr, Xe) are confined along the tubule axis ($R^*<1.22$) and $\Delta V=0$. The adsorption energy significantly decreases with respect to the other situation ($R=5.25$ Å) due to the increase of confinement. Such a feature is particularly striking for the rare gas atoms.

We have finally calculated the vibrational frequencies ω_r connected to the motions of the adatoms perpendicularly to the tubule axis (Tables III and IV). These frequencies decrease significantly when the metal-ion size increases. For the rare gas atoms, these frequencies are small, indicating that the shape of the potential well is relatively flat around the equilibrium, although the adsorption well is generally deep in tubes. A different situation occurs for the Buckyballs due to the enhanced confinement in a sphere, and the corresponding frequencies are higher as shown for the lighter rare gas atoms in C_{60} (Table V and Fig. 4).

To conclude this section, the calculations show that the endohedral adsorption of rare-gas atoms and alkali-metal ions can be easily studied on the basis of the general results obtained in Secs. III–VI. These molecular species are good candidates for adsorption in the most probable nanotubes, which obey the conditions required for the application of continuum approximation and in some cases of the geometrical confinement.

TABLE IV. Adsorption characteristics for various atoms in a carbon tubule with radius 4 Å.

			V_m (meV)		$\Delta V = V(0) - V_m$ (meV)		
X	R^*	r_m (Å)	$N=1$	$N=4$	$N=1$	$N=4$	ω_r (cm^{-1})
Li^+	1.90	1.86	−730	−821	450	481	441
Na^+	1.60	1.43	−709	−796	257	274	173
K^+	1.37	0.92	−775	−866	81	88	89
He	1.32	0.76	−44	−49	2.5	2.7	45
Ne	1.26	0.50	−84	−94	1.1	1.3	23
Ar	1.16	0	−257	−284	0	0	25
Kr	1.13	0	−317	−350	0	0	25
Xe	1.04	0	−429	−482	0	0	47

TABLE V. Radial vibrational frequencies ω_r (cm^{-1}) for rare gas @$C_{m,n}$ (single-shell tube with $R=3.55$ Å) and rare gas @C_{60}.

Rare gas	@$C_{m,n}$	@C_{60}
He	37	70
Ne	40	65
Ar	80	120

VIII. CONCLUSION

Carbon nanotubes are clearly container compounds which can be considered with a good accuracy as continuum media for some encapsulated atoms and molecules. In principle, they may be tailored to incarcerate guest molecules with different shapes and sizes. An appropriate selection of the tube diameter for a given molecular species would result in a withdrawing of the molecules collinear with the tube axis, as shown in this paper. Although the encaged systems considered here appear too simple and the ingredients used require some improvements (regarding the potential forms, the influence of the tube caps,...), these results could be at the basis of a more general study of processes associated with the unidimensional physics and chemistry. Low dimensional reactivity of molecules in tubes, catalysis and wetting properties inside cylindrical nanostructures and also chirality discrimination of chiral molecules in $C_{m,n}$ tubes (m or $n\neq 0$) are some examples of this potentiality.

ACKNOWLEDGMENT

The authors gratefully acknowledge a partial financial support of this work by the Consejeria de Educacion del Gobierno Autonomo de Canarias (Project PI 92/077).

[1] W. E. Billups and M. A. Ciufolini, *Buckminsterfullerenes* (VCH, New York, 1993).
[2] S. Iijima, Nature **354**, 56 (1991).
[3] T. W. Ebbesen and P. M. Ajayan, Nature **358**, 220 (1992).
[4] Y. Saito, T. Yoshikawa, S. Bandow, M. Tomita, and T. Hayashi, Phys. Rev. B **48**, 1907 (1993).
[5] S. Iijima and T. Ichihashi, Nature **363**, 603 (1993).
[6] D. S. Bethune, C. H. Klang, M. S. de Vries, G. Goman, R. Savoy, J. Vazquez, and R. Beyers, Nature **363**, 605 (1993).
[7] D. S. Bethune, R. D. Johnson, J. R. Salem, M. S. de Vries, and C. S. Yannoni, Nature **366**, 123 (1993).
[8] S. C. Tsang, P. J. F. Harris, and M. L. H. Green, Nature **362**, 520 (1993).
[9] P. M. Ajayan, T. W. Ebbesen, T. Ichihashi, S. Iijima, K. Tanigaki, and H. Hiura, Nature **362**, 522 (1993).
[10] P. M. Ajayan and S. Iijima, Nature **361**, 333 (1993).
[11] R. S. Ruoff, D. C. Lorents, B. Chan, R. Malhotra, and S. Subramoney, Science **259**, 346 (1993).
[12] S. Seraphin, D. Zhou, J. Jiao, J. C. Withers, and R. Loutfy, Nature **362**, 503 (1993).
[13] S. I. Sawada and N. Hamada, Solid State Commun. **83**, 917 (1992).
[14] A. A. Lucas, P. H. Lambin, and R. E. Smalley, J. Phys. Chem. Solids **54**, 587 (1993).
[15] M. S. Dresselhaus, G. Dresselhaus, and R. Saito, Solid State Commun. **84**, 201 (1992).
[16] N. Hamada, S. Sawada, and A. Oshiyama, Phys. Rev. Lett. **68**, 1579 (1992).

[17] C. T. White, D. H. Robertson, and J. W. Mintmire, Phys. Rev. B **47**, 5485 (1993).
[18] R. A. Jishi, M. S. Dresselhaus, and G. Dresselhaus, Phys. Rev. B **47**, 16 671 (1993).
[19] M. S. Dresselhaus, G. Dresselhaus, and P. C. Eklund, J. Mater. Res. **8**, 2054 (1993).
[20] R. Saito, M. Fujita, G. Dresselhaus, and M. S. Dresselhaus, Appl. Phys. Lett. **60**, 2204 (1992).
[21] J. W. Mintmire, B. I. Dunlap, and C. T. White, Phys. Rev. Lett. **68**, 631 (1992).
[22] J. Yel-Yi and J. Bernholc, Phys. Rev. B **47**, 1708 (1993).
[23] H. Ajiki and T. Ando, J. Phys. Soc. Jpn. **62**, 1255 (1993).
[24] E. G. Galpern, I. V. Stankevich, A. L. Chistykov, and L. A. Chernozatonskii, Chem. Phys. Lett. **214**, 345 (1993).
[25] M. R. Pederson and J. Q. Broughton, Phys. Rev. Lett. **69**, 2689 (1992).
[26] M. Abramowitz and I. A. Stegun, *Handbook of Mathematical Functions* (Dover, New York, 1970).
[27] D. H. Everett and J. C. Powl, J. Chem. Soc. Faraday. Trans. I **72**, 619 (1976).
[28] J. Breton, J. Gonzalez-Platas, and C. Girardet, J. Chem. Phys. **99**, 4036 (1993).
[29] W. A. Steele, *The Interaction of Gases with Solid Surfaces* (Pergamon, Oxford, 1974).
[30] G. Vidali, G. Ihm, H. Y. Kim, and M. W. Cole, Surf. Sci. Rep. **12**, 133 (1991).
[31] N. D. Shrimpton, M. W. Cole, W. A. Steele, and M. W. C. Chan, in *Surface Properties of Layered Materials*, edited by G. Benedek (Kluwer, Dordrecht, 1992).
[32] W. A. Steele, Chem. Rev. **93**, 2355 (1993).